Preferential Radon Transport Through Highly Permeable Channels in Soils

Mosley, R. B.
USEPA, Office of Research and Development
National Risk Management Research Laboratory
Research Triangle Park, NC 27711

ABSTRACT

Indoor radon levels (that can pose a serious health risk) can be dramatically increased by air that is drawn into buildings through pipe penetrations that connect to permeable channels in soils. The channels, commonly containing gravel bedding around utility pipes, act as a collection plenum for soil radon and can draw air from distances approaching 100 m. Equations characterizing air and radon flow in such channels are developed and compared with field data in this paper. This pollutant entry mechanism has recently attracted new attention because of its relevance to entry of volatile organic compounds from contaminated groundwater, leaking storage tanks, landfills, and other sources of soil vapor contamination.

Three test channels were constructed to simulate conditions associated with utility line installations The channels were constructed in 0.3 m wide trenches at depths of between 0.9 and 1.2 m. A 63 m long channel was filled with clean gravel, and two 30 m long channels were filled with native soil and sand, respectively. The trench volumes above the channels were backfilled with native soil. A suction tube was installed at one end of each channel for pumping air from it, and air sampling tubes were installed at regular intervals along the channel to monitor air pressure distributions and radon concentrations.

Site sampling characterized soil radium, emanation, moisture, particle size, density, specific gravity, permeability, and diffusion coefficient properties. Soils were relatively homogeneous in all respects except for reduced density in the recompacted soil above the channels and slightly reduced moisture in near-surface soils. The soil radon generation rate was 99.9 Bq m^{-3} s^{-1}, compared to 7.4 Bq m^{-3} s^{-1} for the gravel and 29.6 Bq m^{-3} s^{-1} for the sand. The effective permeability of site soils was observed to increase over a 3-month period during the spring and early summer.

Experiments, in which air was extracted through the suction tube, showed that pressures and air flow rates decreased exponentially with distance along each channel, as predicted. Pressure influences in the gravel channel propagated more than 30 m, while those in the soil and sand channels were limited to approximately 5 m. Pressures calculated from independent permeability measurements agreed with measured pressure profiles in the gravel channel within an average of 12%.

Radon concentrations in the channels were lower than in surrounding soil because of their greater porosity and reduced radon source strengths. With constant suction from the end of the gravel channel, radon concentrations within 10 to 20 m of the suction point were diluted by infiltrating surface air despite the increased advective transport of radon from surrounding soils into the channel. The resulting radon profile had concentrations near the outlet that were about 75% of the concentrations at 60 m distance. Calculated concentrations near the outlet averaged within 14% of measured concentrations, and calculated concentrations at the opposite end were within 2% of the measured concentrations. Despite dilution by infiltrating surface air, radon produced by the gravel channel was approximately 12.7 Bq s^{-1}, which is sufficient to produce indoor radon concentrations above 222 Bq m^{-3} in a typical single-story house with a ventilation rate of 0.5 air change per hour.

1. BACKGROUND

Radon (^{222}Rn) gas enters buildings primarily from radium (^{226}Ra) in foundation soils. If the radon entry rate is elevated and the building is not well ventilated, the radon can accumulate to levels that significantly increase the risk of lung cancer in chronically exposed occupants. Their degree of health risk is proportional to their long-term average level of radon exposure. The U.S. Environmental Protection Agency (EPA)[1,2] recommends remedial action if indoor radon levels average 148 Bq m^{-3} (4 pCi L^{-1}) or higher.

Indoor radon concentrations are expected to be proportional to soil radium concentrations. However, the dependence of indoor radon on soil properties is sometimes obscured by factors such as: fluctuating building ventilation rates and air pressures, heterogeneity of soil radon sources and transport rates, and poorly characterized cracks and openings in the building foundation. These complicating effects are sufficiently influential that some empirical studies, when not properly designed, have even failed to show a correlation between indoor radon and soil properties[3]. However, most studies show clear correlation of radon levels with soil properties. Mathematical models[4,5,6,7,8] have helped quantify the amount of radon produced by soils and how it enters houses and accumulates indoors.

Model calculations of soil radon entry have shown excellent agreement[7] with measured data for carefully constructed test structures and for many houses. However, serious discrepancies are also observed in many cases. For example, radon levels in the Lawrence Berkeley Laboratory (LBL) test structures exceeded model calculations by as much as a factor of 8 when soil gas flow was modeled as the only radon entry mechanism[9]. Although radon diffusion can also cause significant radon entry, the LBL data suggest that pressure-driven soil gas flow caused the anomalous radon levels.

Several explanations have been offered for excessive soil gas flow into structures. These include enhanced permeability of backfill soils or heterogeneous layers, anisotropic soil permeability due to sedimentary deposition, and permeable soil channels associated with animal burrows or buried utility lines. While backfill zones and soil layering have been the subject of previous field studies, permeable soil channels are more difficult to find and have generally been ignored.

Mosley[10,11] has developed a mathematical model indicating important contributions from the permeable channels commonly associated with utility pipes. Since the channels connect to houses at pipe penetration points, the houses can potentially draw soil gas from the channels through leaks in the pipe-concrete joint. Soil gas entry from the channel is enhanced by the common use of permeable gravel bedding in pipe trenches. Even when native soil is used to backfill around pipes, it is not ordinarily compacted to achieve a permeability as low as that of the surrounding soil. Mechanical vibrations and temperature changes in the pipe may also create a concentric permeable zone.

The permeable channel model[10] indicates that air movement along pipe channels could account for 50 to 75% of indoor radon concentrations if the channel permeability is approximately 10,000 times that of the surrounding soil. While gravel in pipe channels could readily provide such a permeability difference, the rate of air movement in the channels needs empirical confirmation.

This paper describes a field study aimed at testing the permeable channel model equations for preferential air flow. The study involved construction of test channels in a homogeneous, low-permeability soil and measurement of air pressure and flow distributions in the channels. Radon concentrations were also measured along the channels and in air drawn from the channels for comparison with radon source strengths computed from radium and radon emanation rates in the surrounding soils. The measurements were compared with trends predicted by the permeable channel model to estimate the potential significance of indoor radon entry from air flow along buried utility lines.

The equations characterizing preferential air flow along permeable soil channels are presented in Section 2, along with their implications for indoor radon contributions. The experimental measurements in the permeable channels are described in Section 3, including site characterization, channel construction, and measurement methods. The results of the site characterization and channel air flow measurements are presented in Section 4, followed by model analyses and comparisons with the experimental data in Section 5. Conclusions are summarized in Section 6.

2. PERTINENT EQUATIONS

2.1 Air Flow and Pressure Equations

The rate of air flow and the distributions of air pressures along a permeable channel connected to a house are defined by Mosley[10] for the simplified geometry illustrated in Fig. 1. The definitions assume that homogeneous soil extends infinitely on either side of the channel and from the surface to a depth much greater than the channel depth. The channel is defined as a circular cylinder of infinite length extending from the house with a defined pressure difference relative to the outdoor pressure at the soil surface. The air flow and pressure distributions are derived[10] using Forchheimer's extension of Darcy's law to obtain the following expressions for air flow and pressure as a function of distance from the house-end of the channel:

$$q(z) = -(3\pi b^2 / 2f)sech^2(\alpha z + \delta) \quad (1)$$

and

$$P(z) = (3\mu / 4fk_2\alpha)tanh(\alpha z + \delta)sech^2(\alpha z + \delta) \quad (2)$$

where q = entry flow rate into a short segment of the channel ($m^3\ s^{-1}$),
z = position along the channel from the house (m),
b = radius of the channel (m),
f = Forchheimer constant for the channel fill material ($s\ m^{-1}$),
sech = hyperbolic secant function,
α = $\{k_1 / [b^2 k_2 \ln([h + (h^2 - b^2)^{1/2}] / [h - (h^2 - b^2)^{1/2}])]\}^{1/2}$,
k_1 = air permeability of the soil (m^2),
k_2 = air permeability of the material in the channel (m^2),
h = depth of the channel from the soil surface (m),
δ = $\tanh^{-1}(\{1 - [2f/3\pi b^2]Q_T\}^{1/2})$,
tanh = hyperbolic tangent function,
Q_T = total flow rate through the channel ($m^3\ s^{-1}$),
$P(z)$ = air pressure in the channel at z relative to ambient air pressure (Pa), and
μ = air viscosity (1.85×10^{-5} Pa·s).

The idealized geometry shown in Fig. 1 is used to approximate an experimental configuration as shown in Fig. 2. Experimentally, the cylindrical channel is approximated by a square geometry, and the uniform soil surrounding the channel has been disturbed and re-compacted for construction of the channel. Although Eqs (1) and (2) assume the properties of the undisturbed (region 1) and recompacted (region 1') soils are identical, measurements show these assumptions to be incorrect. An attempt is made to account for such differences by using an effective permeability.

2.2 Equations for Indoor Radon Entry

The amount of radon entry from the permeable channel to the indoor environment is the total amount of radon that gets swept past the $z = 0$ point in the channel. This quantity has been approximated[10] by first computing the radon entry into incremental sections along the length of the channel, and then integrating the amount of radon along the total channel length . The radon activity at the surface of the channel is obtained by solving the steady-state radon transport equation:

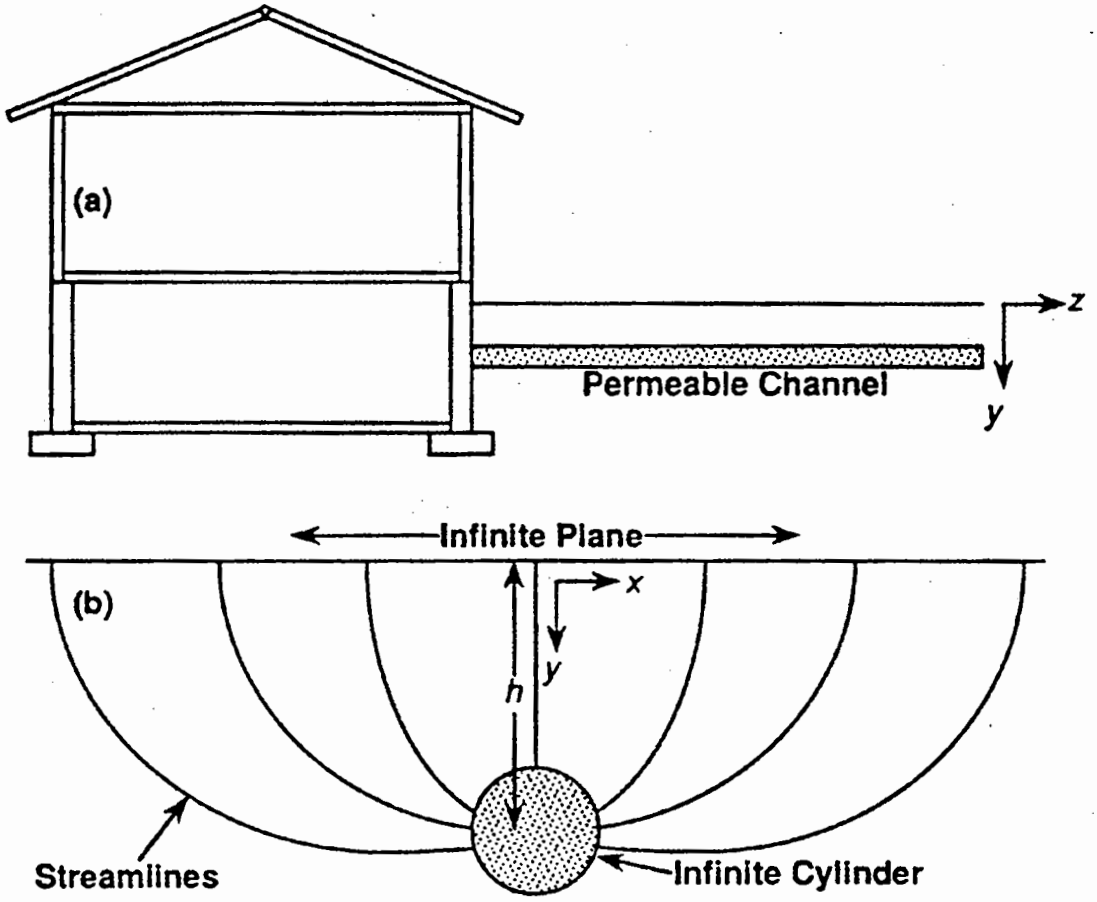

Figure 1. (a) Schematic diagram of a house with a permeable channel connected to a basement entry point, and (b) a cross section of the permeable channel.

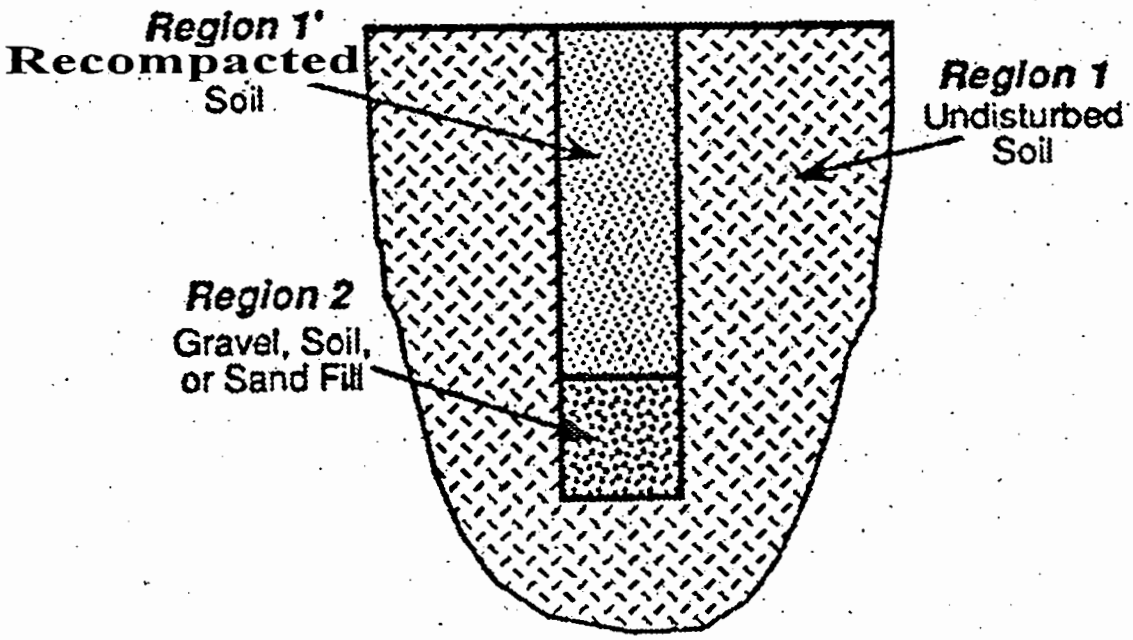

Figure 2. Schematic diagram of experimental channel cross section.

$$D\nabla^2 C - (\vec{v}/\varepsilon)\cdot\nabla C + G - \lambda C = 0 \qquad (3)$$

where D = diffusion coefficient of radon in the pore space ($cm^2\ s^{-1}$),
∇ = gradient operator,
C = radon concentration ($Bq\ m^{-3}$),
$\vec{v}$ = Darcy velocity of gas flow ($m\ s^{-1}$),
ε = soil porosity (dimensionless),
G = radon generation rate ($Bq\ m^{-3}\ s^{-1}$), and
λ = radon decay constant ($2.1 \times 10^{-6}\ s^{-1}$).

The components of air velocity are given by[10]:

$$v_x = \frac{4k_1 P(z)\sqrt{h^2 - b^2}}{\mu \ln[(h+\sqrt{h^2-b^2})/(h-\sqrt{h^2-b^2})]}\left(\frac{2xy}{(h^2 - b^2 + x^2 + y^2)^2 - 4y^2(h^2-b^2)}\right) \qquad (4)$$

and

$$v_y = \frac{-4k_1 P(z)\sqrt{h^2 - b^2}}{\mu \ln[(h+\sqrt{h^2-b^2})/(h-\sqrt{h^2-b^2})]}\left(\frac{h^2 - b^2 + x^2 - y^2}{(h^2 - b^2 + x^2 + y^2)^2 - 4y^2(h^2-b^2)}\right) \qquad (5)$$

where v_x = horizontal air velocity perpendicular to the channel ($m\ s^{-1}$),
x = horizontal distance from the channel (m),
y = vertical distance from the soil surface (m), and
v_y = vertical air velocity perpendicular to the channel ($m\ s^{-1}$).

Eqs (3) to (5) are solved numerically to obtain the radon concentrations in the x-y plane at various values of z. The resulting concentrations at the surfaces of the cylindrical channel are then averaged over its circumference. The rate of radon entry into the building, approximated by the radon entry into the channel, is then obtained by numerically integrating the products of the radon concentrations and air flow velocities into the channel as:

$$Entry = 2\pi b \int_{\infty}^{0} C_s(z) v(z) dz \qquad (6)$$

where *Entry* = radon entry rate ($Bq\ s^{-1}$),
$C_s(z)$ = average radon concentration at the channel surface ($Bq\ m^{-3}$), and
$v(z)$ = average velocity of soil gas entering the channel at z ($m\ s^{-1}$).

As an alternative to the numerical solution of this set of equations, the entry rate is approximated

using advective flow through the recompacted soil and diffusion through the undisturbed soil. A second alternative approach uses similar assumptions to compute the radon concentration in the channel and the entry rate as the product of concentration and flow rate at the building-end of the channel.

2.3 Approximations That Apply for the Experimental Conditions

The experimental conditions, described in Section 3, allow several approximations to be made to Eqs (1) through (6). For example, δ is always greater than approximately 1.75, so that $\tanh(\alpha z + \delta)$ is approximately unity, and $\text{sech}(\alpha z + \delta)$ can be approximated by $2\exp[-(\alpha z + \delta)]$. Making these substitutions into Eqs (1) and (2) gives:

$$q(z) = -Q_T \exp(-2\alpha z) \tag{7}$$

and

$$P(z) = (\mu Q_T / 2\pi b^2 \alpha k_2) \exp(-2\alpha z) \tag{8}$$

A comparison of measured radon concentrations and entry rates with model predictions requires the solution of the multidimensional Eqs (3) through (5), and subsequent integration of Eq (6). In most instances, these solutions would require numerical methods of evaluation. Some analytical approximations have been applied to the Eqs (3) through (5) to obtain approximate closed-form solutions. For the experimental values of h and b, the soil-gas velocity into the channel varies only slightly from the top of the channel to the bottom. Therefore, it is a good approximation to represent the x and y components of the velocity vector [Eqs (4) and (5)] by a radial velocity scaler that is independent of angle in cylindrical coordinates. Therefore, the velocity at the mid-plane of the channel is given by:

$$v_r(z) = \frac{4k_1 P(z)\sqrt{h^2 - b^2}}{h^2 \mu \varepsilon \ln[(h + \sqrt{h^2 - b^2}) / (h - \sqrt{h^2 - b^2})]} \tag{9}$$

where $v_r(z)$ = radial air velocity perpendicular to the channel at z (m s^{-1}).

The $v_r(z)$ is obtained from the sum of the squares of Eqs (4) and (5). The velocity given by Eq (9) is the linear velocity, not the Darcy velocity. The average velocity, $v_z(z)$, inside the channel is readily obtained from Eq (7) after dividing by the cross sectional area to give:

$$v_z(z) = v_z(0) \exp(-2\alpha z) \tag{10}$$

where $v_z(0) = - Q_T/(\pi b^2)$.

An approximate solution to eqs (3) through (5) is obtained by using eq (9) in an approximate version of eq (3). As will be shown in Section 4, the permeability of the backfill soil over the channels is greater than the permeability of the undisturbed native soil. This causes the advective flow into the channel to be mainly from flow through the backfill soil, so that this advective transport can be approximated over a small segment of the top surface. Furthermore, the air velocity in the backfill soil near the suction point is sufficiently high that the diffusive term in this region can be neglected. Transport through the rest of the soil around the channel is mainly by diffusion, so the transport in this undisturbed-soil region can be approximated by the analytical solution to the two-region, infinite-medium cylindrical diffusion equation. This solution contains the modified Bessel functions I_0, I_1, K_0, and K_1. For the region of interest around the channel, these Bessel functions can be represented by their asymptotic approximations. The resulting advective and diffusive expressions can be combined to give:

$$C_b(z) = [\frac{G_2 / \lambda + (2/b)\sqrt{D_1 / \lambda} G_1 / \lambda}{1 + (2/b)\sqrt{D_1 / \lambda}}][1 - \frac{1}{3}\exp(-\lambda \varepsilon \pi h^3 e^{2\alpha z} / Q_T)] \quad (11)$$

where

$C_b(z)$ = average radon concentration in the channel (Bq m^{-3}),
G_1 = radon generation rate in region 1 (Bq m^{-3} s^{-1}), and
G_2= radon generation rate in region 2 (Bq m^{-3} s^{-1}).

The 1/3 factor in the last term in brackets exceeds 1/4th of the channel circumference because the depleted concentration from advection is assumed to decrease the channel boundary radon concentration near the advective zone. This depletion zone in the diffusion component of the concentration was assumed to increase linearly for two diffusion lengths on each side of the advective zone.

Eq (6) assumes that the radon entry rate into a building equals the advective radon entry rate through the walls of the channel. This assumption neglects diffusive entry through the walls of the channel as well as decay while radon is in transit in the channel. An analytical solution to eqn (6) is obtained by using eqs (9) and (11). The resulting expression is:

$$Entry_a = \frac{2bQ_T}{\varepsilon h \lambda}[\frac{G_2 + (2/b)\sqrt{D_1 / \lambda} G_1}{1 + (2/b)\sqrt{D_1 / \lambda}}][1 - \frac{1}{6}\exp(-\lambda \varepsilon \pi h^3 e^{2\alpha z} / Q_T)] \quad (12)$$

A simpler and more direct expression for the entry rate is the product of the average channel radon concentration and the axial velocity at $z = 0$. Using eqs (10) and (11), this product gives:

$$Entry_b = \frac{Q_T}{\lambda}[\frac{G_2 + (2/b)\sqrt{D_1 / \lambda} G_1}{1 + (2/b)\sqrt{D_1 / \lambda}}][1 - \frac{1}{3}\exp(-\lambda \varepsilon \pi h^3 / Q_T)] \quad (13)$$

Both Eqs (12) and (13) were derived for comparison to the experimental data.

The radon generation rate, G, in a given medium is defined as:

$$G = R\rho E\lambda / \varepsilon \qquad (14)$$

where R = radium concentration (Bq kg^{-1}),
ρ = dry density (g cm^{-3}),
E = radon emanation coefficient (the fraction of decaying radium atoms that result in radon atoms suspended in the gas phase),
ε = material porosity (fraction) = 1 - ρ/ρ_g , and
ρ_g = specific gravity (g cm^{-3}).

3. EXPERIMENTAL DESIGN AND MEASUREMENTS

A set of permeable test channels was constructed for measuring air flow and pressure distributions to compare with the predictions from Eqs (1) and (2). This section describes the characterization of the site, the design and construction of the channels, and the measurements that were conducted on the completed channels.

The selected site had favorable permeability properties, and was also observed to have adequate size, level surface topography, uniform clayey textures, favorable location, and possibly adequate soil thickness. In further investigations, soil samples collected at the east, center, and west areas of the site were tested for moisture content and radium concentration. The moisture averaged 25.8 ± 3.7%, and the radium concentrations averaged 80.1 ± 18.5 Bq kg^{-1}. The high moisture was typical of the clayey soil texture, and the radium concentrations were sufficiently high to generate measurable radon concentrations even during channel air flow experiments.

3.1 Channel Construction

Three permeable channels were constructed at the site spanning a permeability range from 10^{-14} to 10^{-8} m^2. Fig. 3 illustrates the cross section of each channel. The channels were constructed by excavating 0.3-m wide trenches to depths of 1.2 m. The lengths and layouts of the trenches at the site are illustrated in Fig. 4. Soils removed from each trench were placed at its side for later use as backfill. After trench excavation, a 0.3-m layer of gravel, native soil, or sand was installed in each trench, as illustrated in Fig. 3. A sheet of permeable, woven geomembrane was then installed over the gravel and sand layers to protect against infiltration of the clayey fill soil.

Air suction and sampling tubes were next installed in the trenches. At the east end of each trench, a metal duct fitting was installed to connect a flexible plastic tube to the 0.3-m square cross section of the fill material, as shown in Fig. 5. The duct fitting was filled with gravel, sand, or soil from the adjoining channel. Air sampling tubes (1.2-m long, 6-mm diameter polyethylene) were then installed into the center of each section of channel fill as shown in Figs. 3 and 5 at the locations indicated in Fig. 4.

Native soil was finally placed back into the trenches and compacted with a 0.3 x 0.3-m power compactor. Final compaction of the soil was augmented by driving over the surface with the excavation backhoe. The ends of all tubes were kept sealed except when connected to pump, sampling, or pressure measurement fittings. The finished channels were allowed to equilibrate and

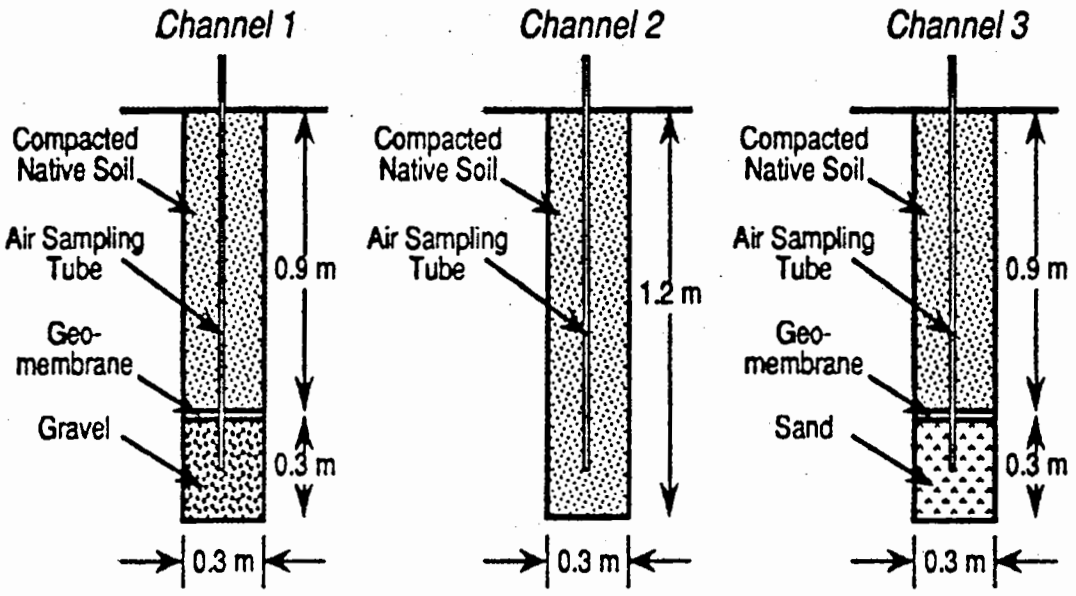

Figure 3. Cross section of the three permeable channels.

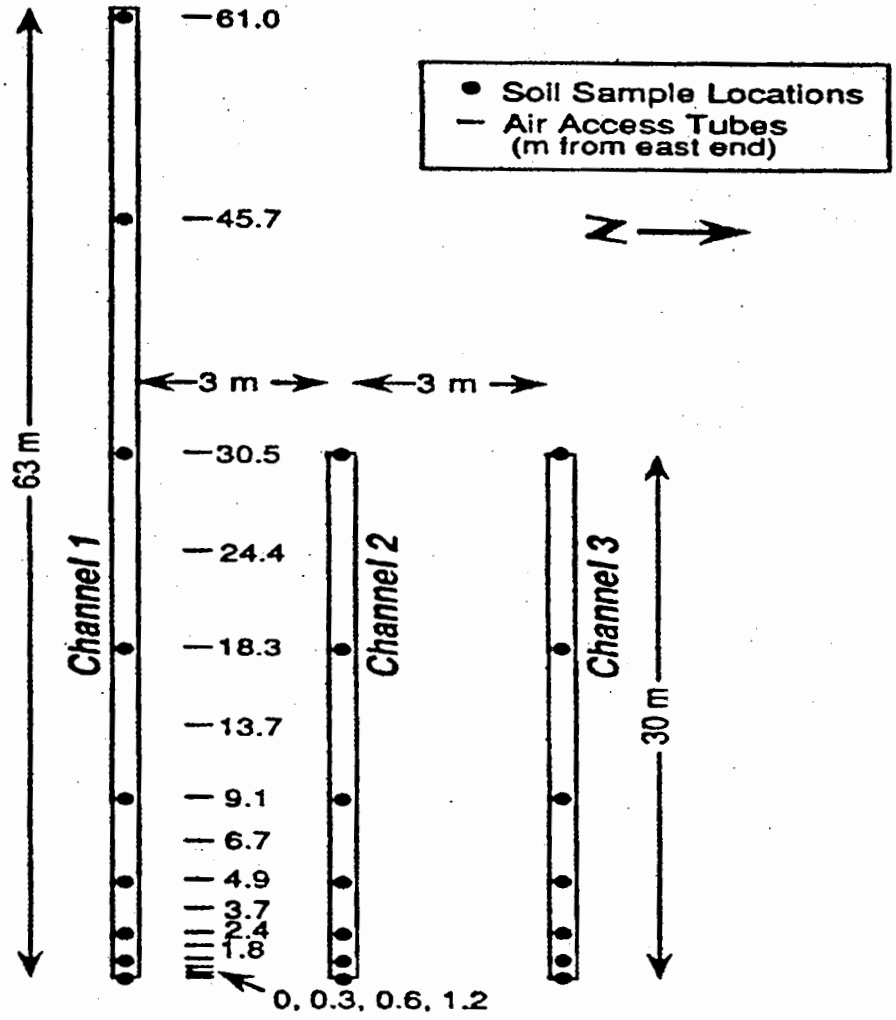

Figure 4. Relative locations of the sampling positions and air access tubes along the channels.

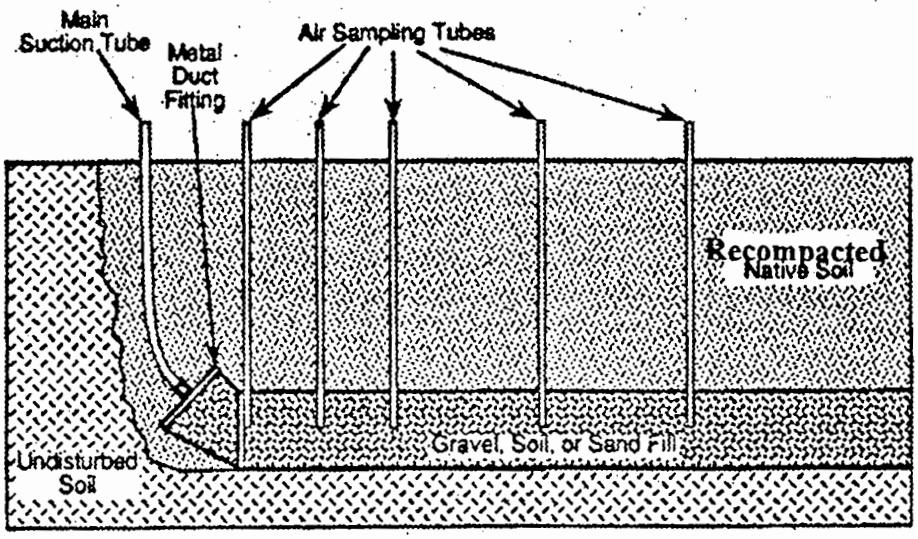

Figure 5. Construction diagram of the channel and air sampling tubes.

settle for approximately 90 days after construction, during which time the site was generally covered with snow.

3.2 Site Description and Characterization

A single boring was completed to a depth of 2.7 m to investigate the extent of the clayey surface soils. The boring utilized a 5-cm diameter soil auger (model 405.23, Arts Manufacturing & Supply, American Falls, ID). Visual observations of soils from the auger cuttings indicated moist clayey soils with no prominent layering throughout the entire profile. The borehole was logged with a gamma scintillation detector (Model 44-3, Ludlum Measurements, Inc., Sweetwater, TX) to estimate the relative distribution of radium and thorium activities. The gamma logging was limited to a depth of 2.2 m by the detector cable length.

Extensive soil sampling utilized soils excavated from trenches during construction of the permeable channels. As illustrated in Fig. 4, samples were collected at nine locations in the first trench and at seven locations in the other two trenches. The soil sampling locations were spaced closer together at the east end, where air pumping and pressure measurements were planned to emphasize the material properties more than those at the more distant locations. At each sampling location, soils were collected to represent three different depth intervals: 0 to 0.4 m, 0.5 to 0.8 m, and 0.9 to 1.2 m. Therefore, a total of 69 samples were collected to characterize the soils around the test channels. Each sample was immediately sealed in a polyethylene bag for storage pending laboratory compositing and analysis. Triplicate samples were also collected from the gravel and sand materials hauled to the site for filling the permeable channel sections of the trenches.

Laboratory analyses included measurements of soil radium concentration, radon emanation coefficient, moisture, density, specific gravity, and particle size distribution. Soil radium, radon emanation, and moisture measurements were performed on 35 individual soil samples, four composite soil samples, and the triplicate sand-and-gravel-fill samples using a previously validated protocol[12]. Triplicate density measurements for the sand and gravel utilized standard laboratory Proctor compaction equipment. Soil density was determined from two *in-situ* samples of undisturbed soils and from three *in-situ* samples of recompacted soils using the drive-cylinder method[13]. Specific gravity was measured on seven soil samples and single sand-and-gravel samples by displacement techniques[14]. Particle size distributions were measured by both sieve and hydrometer methods[15] on six soil samples and single sand-and-gravel samples.

The radon diffusion and air permeability properties of the gravel, soil, and sand were also measured for use in radon generation and transport modeling. Since these properties depend on both density and moisture, estimated conditions for each material were used in performing the laboratory tests. The radon diffusion coefficients were measured using the transient-diffusion method reported previously[16]. The air permeability constants were determined from air pressure/flow data from 10-cm diameter laboratory tubes packed with the gravel or sand samples. Air pressure and flow measurements over an extended range were also used to determine the Forchheimer constant for the gravel[10]. Laboratory air permeability measurements were not attempted for the site soils, since *in-situ* permeability measurements were planned to coincide with the field studies of the completed channels.

3.2.1 Soil Air Permeability

The air permeability of soils at the channel site was initially measured in April 1995 at three depths using driven probes (Type GP, Rogers & Associates Engineering Corp., Salt Lake City, UT). The probes were connected to a permeameter that measured suction pressures and flow rates of air drawn from the soil (Model MK-II Radon/Permeability Sampler, Rogers & Associates). The calibration and method for computing soil permeability from the pressure/flow data are reported

elsewhere[17]. Because of suspected soil drying during the April-June time period, additional soil permeability measurements were conducted in June 1995 by the same method upon completion of the channel air pressure/flow tests. The air permeability in the recompacted soils over the channels was measured separately from that of the undisturbed soils.

Moisture profiles in undisturbed soils were measured by sampling two 1.5-m boreholes in early April 1995. Soil boring utilized the same equipment and methods as for the site characterization boring described in Section 3.2. Subsequent surface samples were collected from backfill and undisturbed soil locations for moisture measurements at the completion of field measurements in June 1995.

3.2.2 Channel Air and Radon Dynamics

The air flow dynamics of the channels were characterized by monitoring air pressures at the various sampling tubes while a vacuum pump drew air from the main suction tube. An in-line flow meter (RMA Series, Dwyer Instruments, Inc., Michigan City, IN) was used between the vacuum pump and the main suction tube to monitor total channel air flow rates. Flow rates between 20 and 70 L min^{-1} were achieved by a carbon-vane pump or a shop vacuum cleaner to characterize the pressure/flow properties of the channels. Air pressures along the channel were measured by successively attaching the air pressure gauge manifold of an MK-II unit to each tube and reading the suction pressure from the most sensitive gauge.

The total radon production rates of each channel were measured by monitoring radon concentrations in the effluent air drawn through their main suction tubes. The radon concentrations were monitored by circulating a fraction of the air from the main suction tube through an alpha scintillation cell (110A, Pylon Electronics, Inc., Ottawa, ONT, Canada) attached to a continuous radiation monitor (AB-5, Pylon Electronics, Inc.). The radon monitor was attached between the flow meter and vacuum pump on the main suction tube, and utilized its internal vacuum pump to sample a fraction of the effluent air stream. Alpha scintillation counts were recorded at regular intervals of 0.5, 1, 2, or 5 minutes. Radon concentrations were calculated from the alpha count rates using the calibration method and equations of Thomas and Countess[18].

In a separate experiment with the gravel channel, radon concentrations were measured at the various locations along the channel during constant pumping of 70 L min^{-1} of air from the channel. For comparison, radon was also measured at several of the channel locations before the pumping had disturbed the channel radon distribution. The radon measurements involved successive connection of the radon monitor to different air sampling tubes and monitoring radon over five 1-minute intervals (1-L min^{-1} air sampling rate). The 70 L min^{-1} channel suction pump was operated for 90 minutes before radon measurements were taken to allow the radon distribution to approach a steady-state condition.

4. RESULTS

This section presents the results of the site characterization and test channel measurements. The site characterization measurements established the fundamental properties of the native soil and channel fill materials at the test site. These provided an important basis for calculating the flow and radon dynamics of the channels. The channel measurements of pressure/flow and radon production properties provide an empirical benchmark for comparison with the model predictions.

4.1 Site Characterization

Results from gamma ray measurements in a borehole are presented in Fig. 6. They show relatively uniform gamma activities even to a depth of 2.2 m. Measurements near the surface are lower because there is less soil above these points (2 vs. 4π solid angle), but are otherwise consistent with the relatively uniform profile for the subsurface depths. The geometric standard deviation of 1.076 indicates less than 8% relative variation among the radioactivity levels at different depths. Since radium activities were found to significantly exceed thorium activities at this site, the gamma ray log also suggests a relatively uniform radon source throughout the 2.2-m soil layer that contains the 1-m deep test channels.

The radium, radon emanation, and moisture measurements on the site soils were averaged by vertical layer, by trench, and by position from the east end of the trench to estimate the site uniformity in all three dimensions. The results of these uniformity estimates are summarized in Fig. 7. As illustrated, there are no clear trends in the horizontal distributions of any of the parameters, nor in the vertical distribution of radium concentrations.

The site averages of all of the radium, radon emanation, and moisture measurements are presented in Table 1. The soil radium concentrations exhibit remarkable uniformity, with an overall relative standard deviation among all of the measurements of only 18%. The soil radon emanation coefficients are distributed somewhat more widely, with an overall relative standard deviation of 25%. Soil moistures had a relative standard deviation of only 14%. The radium concentrations, radon emanation coefficients, and moistures in the gravel and sand were considerably lower than in the clayey soil, as would be expected.

Table 1. Site-Average Properties of Soil and Fill Materials.[a]

Material	Radium ($pCi\ g^{-1}$)	Radon Emanation (fraction)	Moisture (% dry mass)	Dry Density ($g\ cm^{-3}$)	Specific Gravity ($g\ cm^{-3}$)
Gravel	0.6 ± 0.1 (3)	0.05 ± 0.01 (3)	2.4 ± 0.1 (3)	1.51 ± 0.03 (3)	2.61 (1)
Soil	2.1 ± 0.4 (47)	0.16 ± 0.04 (45)	27.5 ± 3.9 (35)	1.59 ± 0.06 (2)	2.70 ± 0.02 (7)
Sand	1.0 ± 0.1 (3)	0.07 ± 0.01 (3)	5.8 ± 0.2 (3)	1.77 ± 0.02 (3)	2.68 (1)

[a]Mean ± standard deviation (number of measurements in parentheses).

The particle size distributions of the gravel, soil, and sand materials were measured. The gravel was predominantly 5 to 15 mm in diameter, with no sands or finer material. The soil was mostly clay, distributed between <0.001 and 0.1 mm in diameter. The sand was narrowly distributed between 0.1 and 5 mm, with approximately 5% clay.

The results of the radon diffusion measurements are summarized in Fig. 8. The respective moistures used for the gravel and sand measurements (0.0 and 5.6%) are similar to field values (2.4 and 5.8%, from Tables 1 and 4), and are not sufficiently different to significantly affect the radon diffusion coefficients[19]. The moistures for the soil radon diffusion measurements at saturation correspond most closely to the average field moistures in Table 1, which also correspond to a

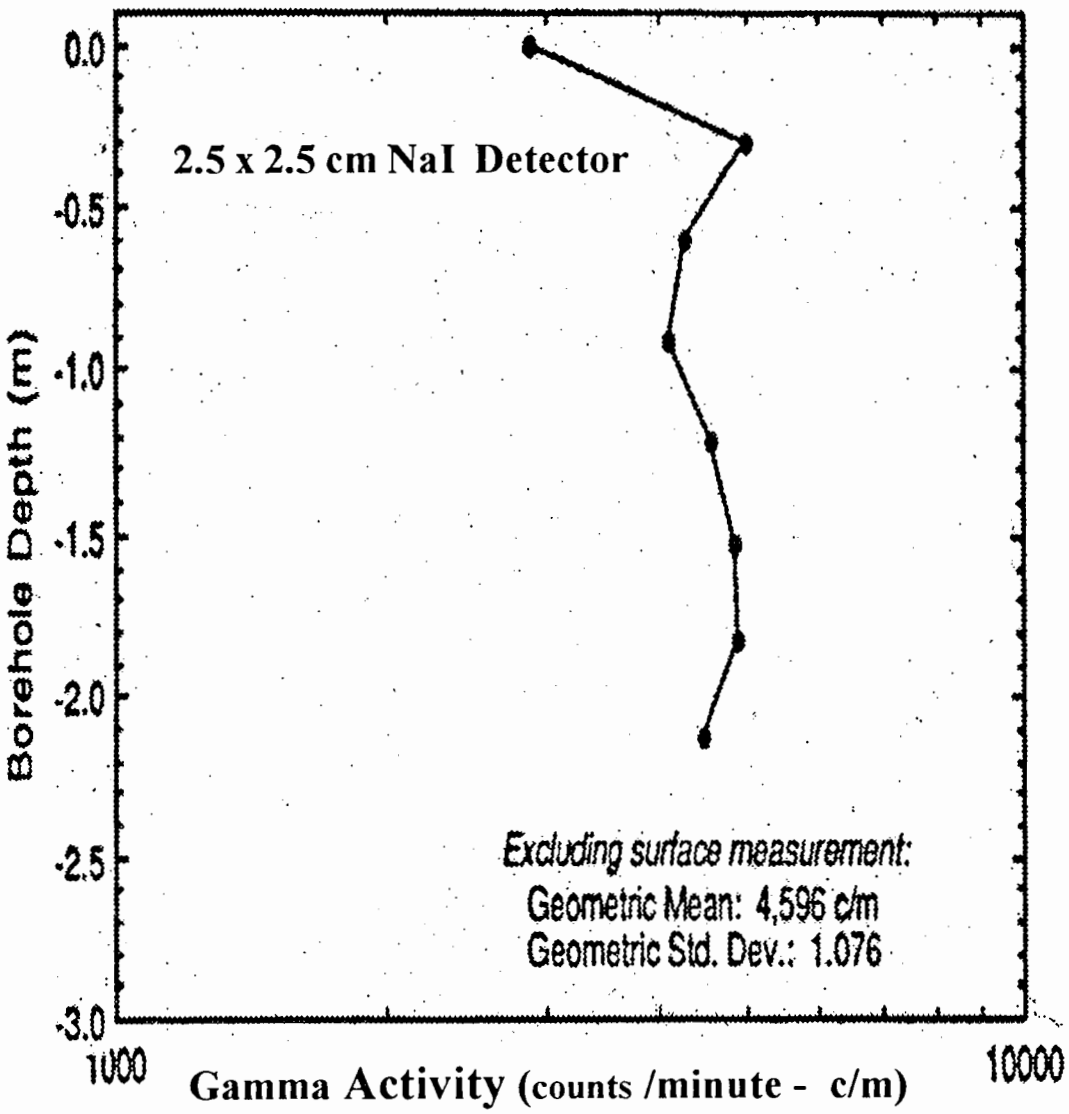

Figure 6. Depth in the borehole versus gamma activity.

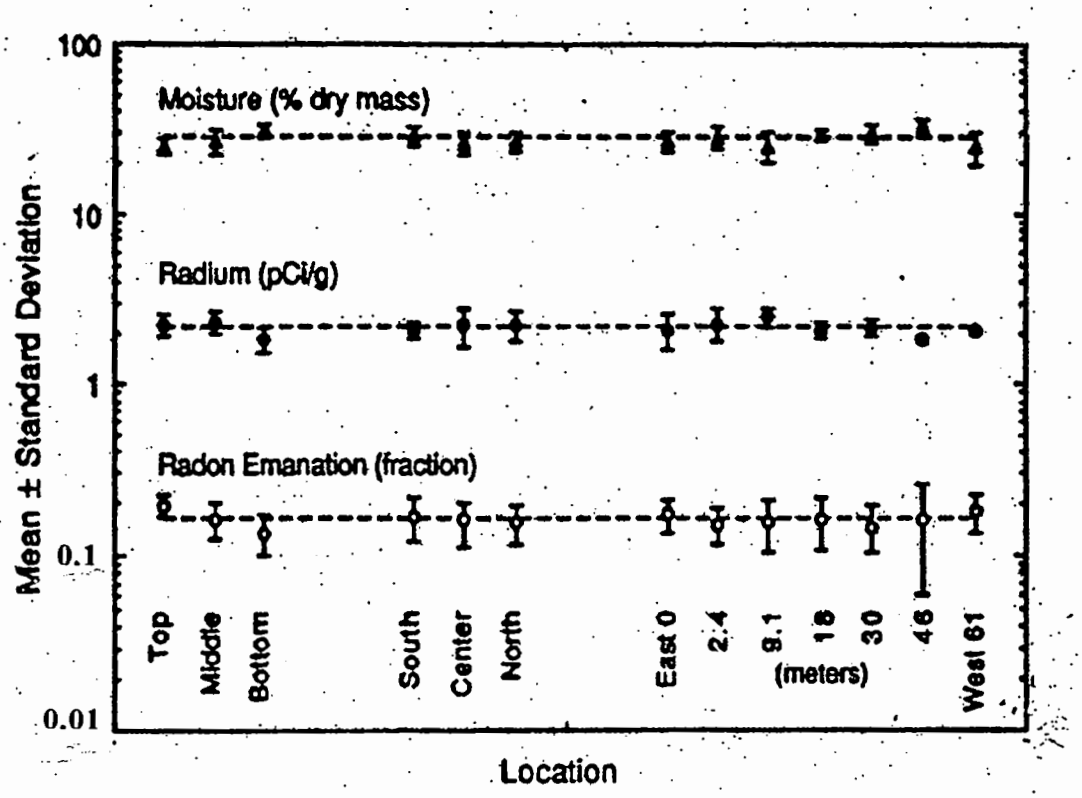

Figure 7. Three-dimensional variations in the means of the radium, radon emanation, and moisture measurements.

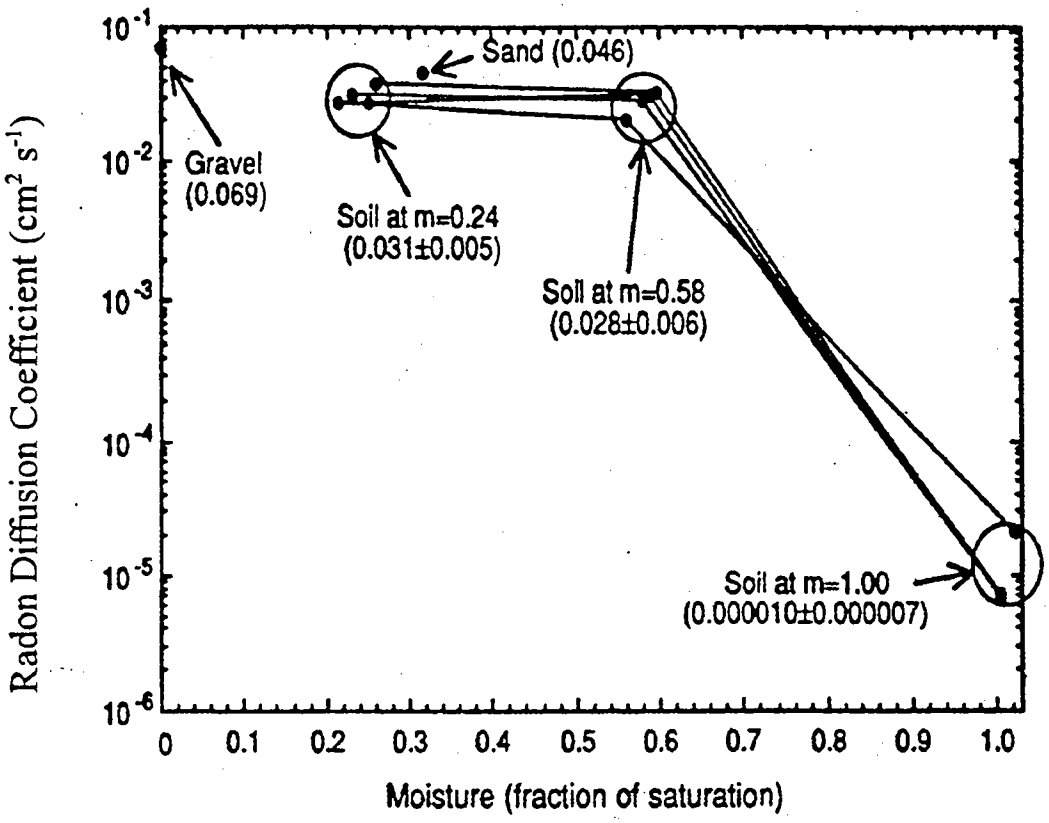

Figure 8. Radon diffusion coefficients as a function of moisture.

correspond most closely to the average field moistures in Table 1, which also correspond to a saturation condition. Therefore, the radon diffusion coefficient for the undisturbed soils is approximated from Fig. 8 by the value $1.0 \times 10^{-5} \pm 7 \times 10^{-6}$ cm^2 s^{-1}.

The initial laboratory air permeability measurements for the gravel and sand materials averaged $6.2 \times 10^{-8} \pm 8.2 \times 10^{-9}$ m^2 and $4.1 \times 10^{-11} \pm 3.5 \times 10^{-12}$ m^2, respectively. The sample moistures for these measurements were similar to those used for the diffusion measurements. The Forchheimer constant was determined from laboratory permeability measurements made on the gravel over a wide range of air pressures and flow rates. These measurements were used to compute an average air permeability of 5.4×10^{-8} m^2 with a Forchheimer factor of 13.7 m s^{-1}.

The first set of *in-situ* air permeability measurements made in the undisturbed site soils is summarized in Table 2. As indicated, the measurements were very narrowly distributed around the overall mean of $4 \times 10^{-14} \pm 9 \times 10^{-15}$ m^2, with minimal depth and location trends. The final measurements of air permeability showed generally higher values for the undisturbed soils, and much higher values in the recompacted soils over the channels, as shown in Table 3.

Soil moisture profiles analyzed in early April 1995 showed a moisture depletion at the 0.3-m depth. Surface samples collected in June 1995 from the 0.1-m depth suggested further depletion in surface soil moisture, particularly in the recompacted soils over the test channels. These observations are consistent with the air permeability measurements in the undisturbed and recompacted soils.

Table 2. Initial *In-situ* Air Permeability of the Site Soils.

Distance from East End (m)	Air Permeability (10^{-14} m^2)			
	0.5 m depth	0.9 m depth	1.2 m depth	Mean ± Std. Dev.
0	7.0	3.9	3.6	4.8±1.9
18	3.9	3.5	3.5	3.6±0.2
34	3.7	4.6	3.4	3.9±0.6
46	3.9	3.7	3.8	3.8±0.1
61	3.4	4.4	3.4	3.7±0.6
Mean ± Std. Dev.	4.4±1.5	4.0±0.5	3.5±0.2	4.0±0.9

Table 3. Final *In-situ* Air Permeability of the Site Soils.

Undisturbed Soils Between Channels		Recompacted Soil over Channels	
Location[a]	Air Permeability (m^2)	Location[b]	Air Permeability (m^2)
C_{1-2} @ 0.9 m	$3.9x10^{-13}$	C_1 @ 0.9 m	$9.3x10^{-11}$
C_{1-2} @ 3.7 m	$7.0x10^{-13}$	C_1 @ 13.7 m	$1.6x10^{-10}$
C_{1-2} @ 63.0 m	$7.0x10^{-13}$	C_1 @ 30.5 m	$2.0x10^{-10}$
C_{1-2} @ 63.0 m	$1.4x10^{-12}$	C_1 @ 61.0 m	$4.7x10^{-10}$
C_{1-2} @ 63.0 m	$6.6x10^{-14}$	C_2 @ 0.9 m	$1.4x10^{-10}$
C_{2-3} @ 0.9 m	$5.8x10^{-13}$	C_2 @ 13.7 m	$2.8x10^{-10}$
C_{2-3} @ 18.3 m	$7.0x10^{-14}$	C_3 @ 0.9 m	$1.4x10^{-10}$
Mean ± Std. Dev.	$(5.6\pm4.7)x10^{-13}$	Mean ± Std. Dev.	$(2.1\pm1.3)x10^{-10}$

[a] C_{m-n} denotes locations between channels m and n at 1 m depth. The position is from the east end of the channels.

[b] C_n denotes locations in channel n at 0.6 m depth. The position is from the east end of the channel.

4.2 Pressure Measurements

The results of the air pressure and flow measurements in the gravel, sand, and soil channels are presented in Figs. 9 through 11, respectively. As illustrated, the air pressures were observed to decrease approximately exponentially with distance from the suction point in all of the channels. Therefore, the measurements are fitted by least-squares regressions to equivalent lines in Figs. 9 through 11 to help identify the pressure-flow characteristics of each channel.

As illustrated by Figs. 9 through 11, the exponents measured for each channel were similar even when different suction pressures were applied. For the gravel channel, the exponents averaged 0.14 ± 0.02 m^{-1}, corresponding to pressure influences as far away as 30 m from the suction point. The exponents for the soil channel were expectedly greater, averaging 0.70 ± 0.19 m^{-1} for a more rapid pressure attenuation within approximately 5 m. However, the exponents for the sand channel were expected to be intermediate, but instead averaged 1.3 ± 0.19 m^{-1}. The intercepts for all of the channels (pressure at z=0) were dependent on the amount of air being pumped from the channels.

The unexpectedly large exponent for the sand channel is attributed to the high permeability of the recompacted soil. The effective permeability of the soil channel exceeded that of the sand by more than a factor of 5. The soil channel propagated suction pressures further because the channel and its cover had similar permeabilities.

5. DISCUSSION AND CONCLUSIONS

The comparisons of measured and calculated channel characteristics focused on the gravel channel because of its large permeability difference from the surrounding soil and its resulting potential for providing useful empirical data. The soil channel was not expected to function as a permeable conduit, but rather as a limiting reference case. The sand channel was also found not to propagate air pressure or flow as far as expected because of the higher permeability of the overlying backfill soil. The following sections summarize the measured properties of the channels and their

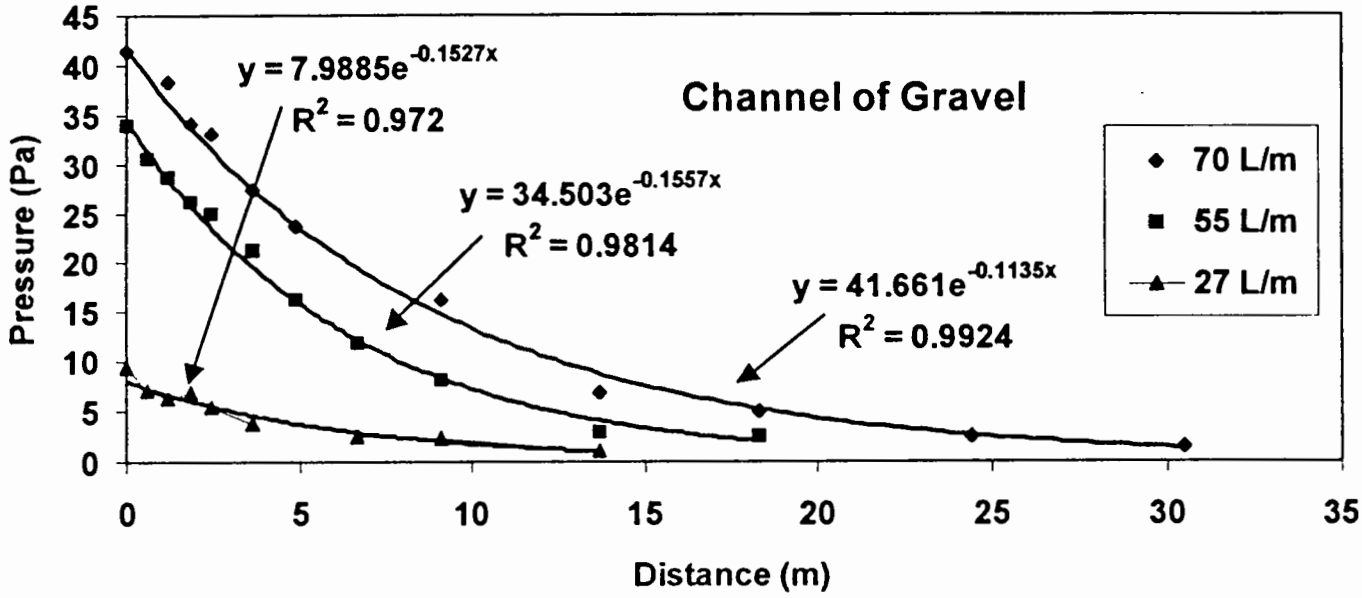

Figure 9. Pressure profiles in the gravel channel.

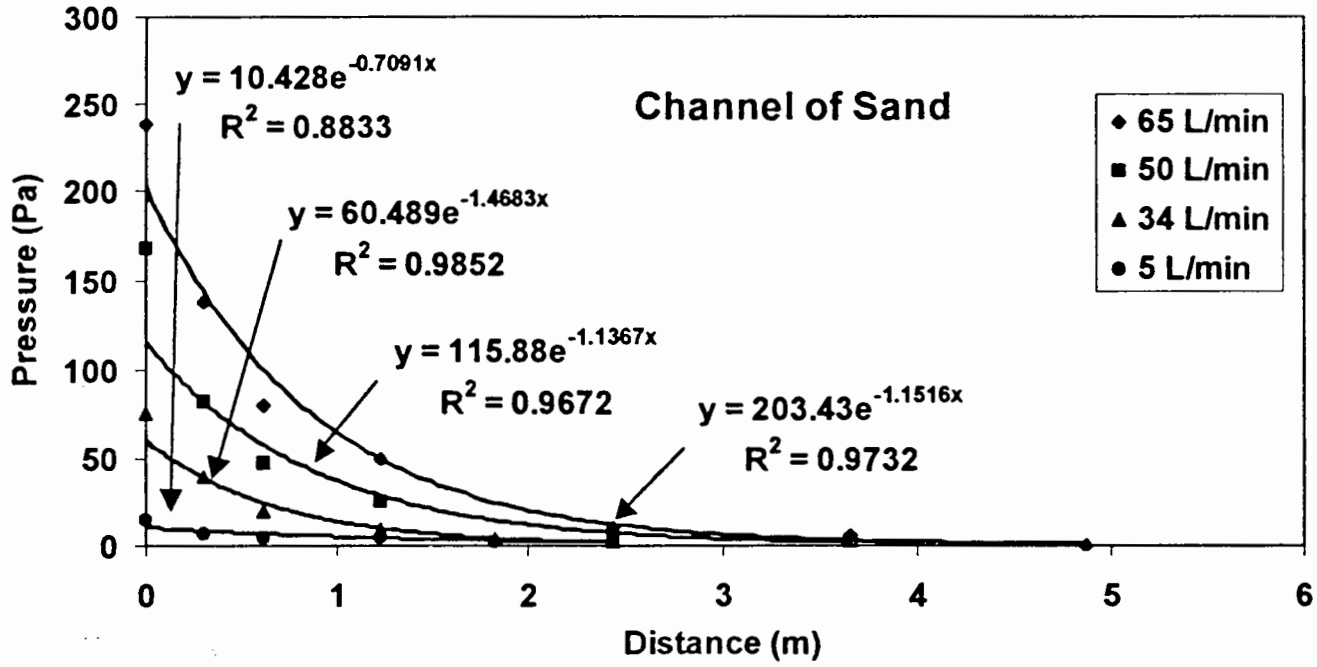

Figure 10. Pressure profiles in the sand channel.

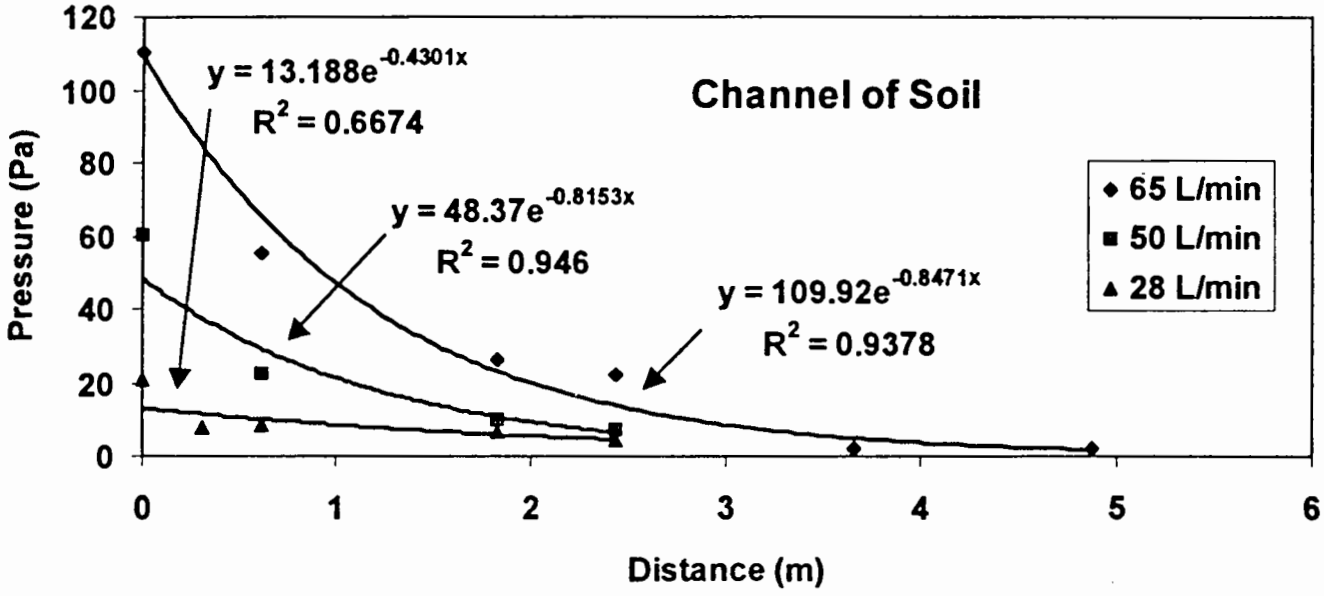

Figure 11. Pressure profiles in the soil channel.

materials and compare the measured air and radon flow characteristics with theoretically calculated values.

5.1 Values of Parameters Used for Model Analyses

Several soil and channel parameters identified earlier must be defined numerically to calculate comparison values for pressure and radon profiles. These parameter definitions are summarized in Table 4. The channel radius, b, was calculated as the radius of a circle with an area equal to that of the 30- x 30-cm channel. The depth, h, was represented by the design depth to the center of the channel. The Forchheimer factor was measured from the non-linear pressure-flow data for channel gravel, but was not determined for the other materials.

Table 4. Summary of Channel Properties.

Parameter (units)	Undisturbed Soil	Recompacted Soil	Gravel	Sand
b (m)	N.A.[a]	0.172	0.172	0.172
h (m)	N.A.	1.07	1.07	1.07
f (s m^{-1})	N.D.[b]	N.D.	13.7	N.D.
R (pCi g^{-1})	2.1	2.1	0.6	1.0
E (fraction)	0.16	0.16	0.05	0.07
ρ (g cm^{-3})	1.59	1.46	1.51	1.77
ρ_g (g cm^{-3})	2.70	2.70	2.61	2.68
ε (fraction)	0.411	0.459	0.578	0.340
M[c] (% dry mass)	25.8	29.9	2.4	5.8
m[d] (fraction)	0.998	0.951	0.0627	0.302
D (cm^2 s^{-1})	1.0×10^{-5}	3.2×10^{-5}	6.9×10^{-2}	4.6×10^{-2}
k (m^2)	5.6×10^{-13}	2.1×10^{-10}	5.4×10^{-8}	4.1×10^{-11}

[a]Not applicable
[b]Not determined
[c]M is % moisture on dry mass basis
[d]$m = \rho M/\varepsilon$ is the fraction of moisture saturation

Radium concentrations and radon emanation coefficients used in Eq (14) were obtained from the measured means in Table 1. The density and specific gravity properties of each material, also obtained from data in Table 1, were used to calculate the porosities listed in Table 4. The respective radon generation rates in the site materials, calculated from Eq (14), were $G_{soil,un} = 0.10$ Bq m^{-3} s^{-1}, $G_{soil,re} = 0.081$ Bq m^{-3} s^{-1}, $G_{gravel} = 0.0059$ Bq m^{-3} s^{-1}, and $G_{sand} = 0.0285$ m^{-3} s^{-1}. These values indicated that the soils were the primary radon sources, and that the sand and gravel fill materials had less significant radon production.

Radon diffusion coefficients were defined directly from the measured values for the sand and gravel, and from the measured mean for the nearly saturated undisturbed soil. For the recompacted soil, the diffusion coefficient was interpolated from the measured values in Fig. 8 at the indicated fraction of moisture saturation. The air permeabilities were defined from laboratory measurements

on gravel and sand, and from field measurements for the soils. The soil permeability measurements in Table 4 are the means of seven measurements each in the undisturbed and recompacted regions.

The measured air pressure profiles shown in Figs. 9 through 11 fit the predicted exponential dependence of pressure on distance given by Eq (8). The least-squares fitting coefficients for the P vs. z data in these figures were therefore used to directly estimate the effective permeability properties of the channels. By substituting the mathematical definition of α and the known values of b and h from Table 4 into Eq (8), expressions were derived to solve for the effective values of k_1 and k_2 for each measured profile. The resulting effective air permeability values are presented in Table 5.

Table 5. Effective Air Permeability of Channel and Soil Materials Computed from Air Pressure Profiles.

Channel Air Flow ($L\ min^{-1}$)	-2α (m^{-1})	Maximum Air Pressure (Pa)	k_1, Soil Air Permeability (m^2)	k_2, Channel Air Permeability (m^2)
Gravel Channel				
27	0.153	7.99	6.4×10^{-11}	7.3×10^{-8}
55	0.156	34.5	3.1×10^{-11}	3.4×10^{-8}
70	0.114	41.7	2.4×10^{-11}	4.9×10^{-8}
Mean			3.9×10^{-11}	5.2×10^{-8}
Standard Deviation			2.1×10^{-11}	2.0×10^{-8}
Soil Channel				
28	0.430	13.2	1.1×10^{-10}	1.6×10^{-8}
50	0.815	48.4	1.0×10^{-10}	4.2×10^{-9}
65	0.847	109.9	6.2×10^{-11}	2.3×10^{-9}
Mean			9.3×10^{-11}	7.6×10^{-9}
Standard Deviation			2.7×10^{-11}	7.6×10^{-9}
Sand Channel				
34	1.47	60.5	1.0×10^{-10}	1.3×10^{-9}
50	1.14	115.9	6.1×10^{-11}	1.3×10^{-9}
65	1.15	203.4	4.6×10^{-11}	9.2×10^{-10}
Mean			6.9×10^{-11}	1.1×10^{-9}
Standard Deviation			2.9×10^{-11}	2.0×10^{-10}

The effective permeabilities in Table 5 are consistent with the more detailed site measurements. Since the recompacted soil region above the channels covers 25% of their perimeter and the undisturbed soil covers 75% of their perimeter, a 3-to-1 weighted average air permeability can be calculated using measurements from Table 4. The resulting effective permeability, 5.3×10^{-11}

m^2, is within 2% of the average empirically fitted value of 5.2×10^{-11} m^2 for the soil around channel 1. Similar permeability values were also obtained for the soils around the other channels. The effective permeability of the gravel in Table 5 is within 4% of the measured value in Table 4. However, there were larger differences between measured and effective fitted values for the soil (27x) and sand (36x) channels. These larger differences were mainly influenced by the proximity of the channel permeabilities with those of the recompacted soils covering the channels.

5.2 Comparison of Measured and Calculated Radon Parameters

The radon concentration profile measured along the gravel channel during an air flow rate of 70 L min^{-1} is illustrated in Fig. 12. For comparison, the average and standard deviation of the radon concentrations in the undisturbed channel before pumping (15910 ± 1850 Bq m^{-3}) is also shown by the straight solid-and-dashed lines. The radon concentrations during pumping approached the undisturbed values at distances of approximately 20 m and greater from the suction point. The depletions at locations closer to the suction point are attributed to dilution by air drawn through the soil above the channel. The vertical error bars correspond to 1 standard deviation from the measured means.

The radon parameters used to compare measurements with theoretical values include radon profiles at different locations along the gravel channel and total radon production rates from the gravel channel. The data used in the calculations are presented in Table 5, and the measured data are shown in the empirical profile in Fig. 12. The calculated radon concentration profile for the gravel channel is shown in Fig. 12 for comparison with the measured profile. Since there was considerable scatter in the data near the origin, the average radon concentration of 10878 Bq m^{-3} for all of the measurements in the first 10 m was compared to the calculated concentration of 9361 Bq m^{-3} for locations near the origin. In this comparison, the calculated concentration is only 14% less than the measured concentration, and is well within the range of experimental variations. At 60 m, near the far end of the channel, the calculated concentration of 14023 Bq m^{-3} is within 2% of the measured concentration. The actual radon profile reaches its maximum in a shorter distance from the origin than the calculated profile.

The experimental rate of radon production by the gravel channel was determined as the product of the measured air flow rate at the origin (1.17×10^{-3} m^3 s^{-1}) and the measured radon concentration at the origin (10878 Bq m^{-3}). This product gave a radon entry rate of 12.7 Bq s^{-1}. The two alternative equations for computing radon entry give $Entry_a$ = 10.6 Bq s^{-1} [from Eq (12)] and $Entry_b$ = 12.3 Bq s^{-1} [from Eq (13)]. The value of $Entry_b$ is about 1% below the measured value, while the value of $Entry_a$ is about 17% below the measured value. Both values are within the estimated experimental uncertainty of the measured value (± 4.07 Bq s^{-1}). As expected from the theoretical derivations, $Entry_a$ is lower than $Entry_b$.

6. SUMMARY AND CONCLUSIONS

Several significant observations were made from this study of preferential radon transport through permeable channels in soils. Some observations concern channel construction, and others concern the physics of air and radon transport into and from the channels.

Channels with up to 10,000 times greater air permeability than surrounding undisturbed soils may be constructed using gravel fill material, but are less likely to be constructed if sand is used in the channel. Even though the channel fill may have the requisite high permeability, trench construction to install the channels disturbs the natural soils enough to increase their air permeability

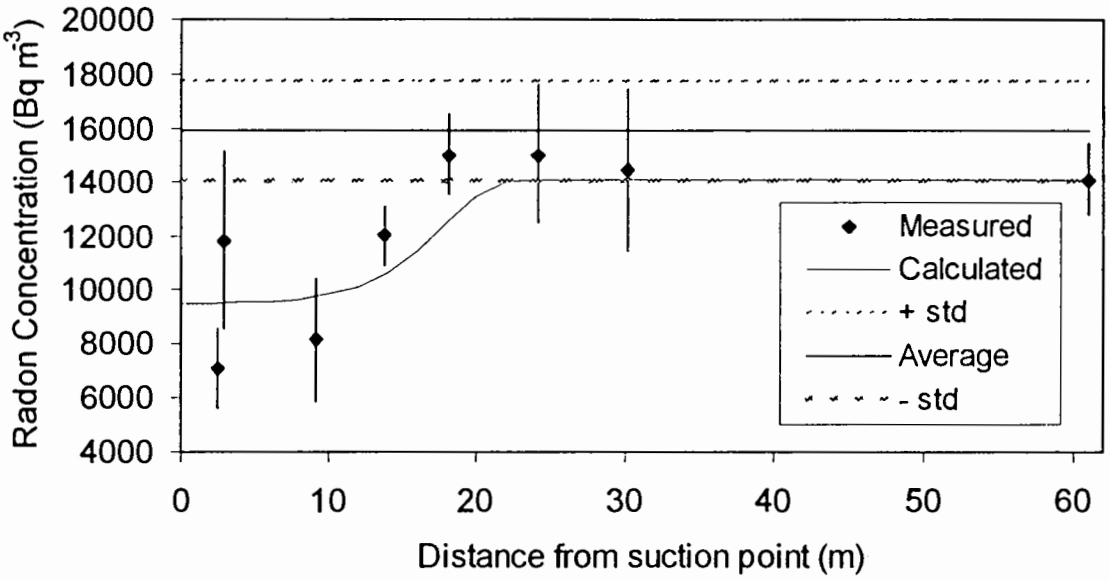

Figure 12. Comparison of measured radon concentrations with model predictions.

by several orders of magnitude. This creates a semipermeable zone of recompacted soil above the channels that limits their air transport distances. Despite standard construction attempts to compact the site soils to their original condition, the air permeability of soils above the test channels increased by more than a factor of 300. The resulting effective permeability of the site soils was still more than 1,000 times lower than the gravel channel material. Although other sites may offer better soil recompaction, the present experience suggests that a factor of 1,000 may be more typical of utility channel permeability ratios than a factor of 10,000.

The pressure distributions along the soil channels were observed to follow exponential decreases from the suction point, regardless of the preferential infiltration of surface air through re-compacted soils. Least-squares regressions of the pressure profiles also provided empirical estimates of the effective air permeability of both channel and surrounding soil materials. These estimates were consistent with direct measurements of site soil permeability and gravel permeability. Measured and calculated pressure distributions in the gravel channel agreed within an average of 4%.

The radon concentrations in the gravel channel were lower than in surrounding soil pores because of the greater pore space and lower radon source strength of the gravel. With constant suction at one end, the radon concentrations in the gravel channel became diluted by infiltrating surface air, despite the increased advective transport of radon from surrounding soils into the channel. The resulting radon profile had concentrations at the channel outlet that were about 75% of the concentrations at a 60 m distance. Most of the depletion occurred in the first 10 to 20 m from the outlet. Calculated radon concentrations near the channel outlet averaged within 14% of measured concentrations, and calculated concentrations at the opposite end of the channel were within 2% of the measured concentration.

Even though significant surface air was drawn into the channel near its exit point, the radon levels were still sufficient to cause elevated indoor radon levels. The radon production rate of the gravel channel was on the order of 12.7 Bq s^{-1}, which is sufficient[7] to cause radon concentrations exceeding 222 Bq m^{-3} (the EPA action level is 148 Bq m^{-3}) in a typical single-story house with a ventilation rate of 0.5 air change per hour.

7. REFERENCES

1. U.S. Environmental Protection Agency, A Citizen's Guide to Radon, second edition, Washington, DC: Office of Air and Radiation, *EPA/402/K-92-001*, May 1992.
2. U.S. Environmental Protection Agency, Technical Support Document for the 1992 Citizen's Guide to Radon, Washington, DC: Office of Radiation Programs, *EPA/400/R-92-011* (NTIS PB 92-218395), May 1992.
3. Nason, R. and B. L. Cohen, Correlation between ^{226}Ra in Soil, ^{222}Rn in Soil Gas, and ^{222}Rn Inside Adjacent Houses, *Health Physics* **52**, 73-77, 1987.
4. Loureiro, C. O., L. M. Abriola, J. E. Martin, and R. G. Sextro, Three-dimensional Simulation of Radon Transport into Houses with Basements under Constant Negative Pressure, *Environmental Science and Technology* **24**, 1338-1348, 1990.
5. Revzan, K. L., W. J. Fisk, and A. J. Gadgil, Modeling Radon Entry into Houses with Basements: Model Description and Verification. Berkeley, CA: Lawrence Berkeley Laboratory report *LBL-27742*, 1991.
6. Swami, M., L. Gu, and V. Vasanth, Integration of Radon and Energy Models for Buildings, Cape Canaveral, FL: Florida Solar Energy Center report *FSEC-CR-617-93*, 1993.
7. Nielson, K. K., V. C. Rogers, V. Rogers, and R. B. Holt, The RAETRAD Model of Radon Generation and Transport from Soils into Slab-on-grade Houses, *Health Physics* **67**, 363-377, 1994.

8. Holford, D.J., Rn3D: A Finite Element Code for Simulating Gas Flow and Radon Transport in Variably Saturated, Nonisothermal Porous Media: User's Manual, Version 1.0, Richland, WA: Pacific Northwest Laboratory report *PNL-8943*, 1994.
9. Garbesi, K., R. G. Sextro, W. J. Fisk, M. P. Modera, and K. L. Revzan, Soil-Gas Entry into an Experimental Basement: Model Measurement Comparisons and Seasonal Effects, *Environmental Science and Technology* **27**, 466-473, 1993.
10. Mosley, R. B., A Mathematical Model Describing Radon Entry Aided by an Easy Path of Migration Along Underground Channels, paper VIP-3, Proceedings, The 1992 International Symposium on Radon and Radon Reduction Technology, Minneapolis, MN, 1992.
11. Mosley, R. B., Model Based Pilot Scale Research Facility for Studying Production, Transport, and Entry of Radon into Structures, paper VI-8, Proceedings, The 1992 International Symposium on Radon and Radon Reduction Technology, Minneapolis, MN, 1992.
12. Nielson, K. K. and V. C. Rogers, A Sensitive Effluent Method for Measuring Radon Gas Emanation from Low-Emanating Materials, *Nuclear Instruments and Methods in Physics Research A*, **353**, 519-523, 1994.
13. ASTM, Standard Test Method for Density of Soil in Place by the Drive-Cylinder Method, Philadelphia, PA: American Society for Testing and Materials, test D2937-83, 1984.
14. ASTM, Standard Test Method for Specific Gravity of Soils, Philadelphia, PA: American Society for Testing and Materials, test D854-83, 1984.
15. ASTM, Standard Method for Particle-Size Analysis of Soils, Philadelphia, PA: American Society for Testing and Materials, test D422-63, 1963.
16. Nielson, K. K., D. C. Rich, and V. C. Rogers, Comparison of Radon Diffusion Coefficients Measured by Transient-Diffusion and Steady-State Laboratory Methods, Washington, DC: U. S. Nuclear Regulatory Commission report *NUREG/CR-2875*, 1982.
17. Nielson, K. K., M. K. Bollenbacher, and V. C. Rogers, User's Guide for the MK-II Radon/Permeability Sampler, Salt Lake City, UT: Rogers & Associates Engineering Corp. report *RAE-9000/9-2*, 1989.
18. Thomas, J. W. and R. J. Countess, Continuous Radon Monitor, *Health Physics* **36**, 734-738, 1979.
19. Rogers, V. C. and K. K. Nielson, Correlations for Predicting Air Permeabilities and ^{222}Rn Diffusion Coefficients of Soils, *Health Physics* **61**, 225-230, 1991.

NRMRL-RTP-P-682

TECHNICAL REPORT DATA
(Please read Instructions on the reverse before completing)

1. REPORT NO. **EPA/600/A-02/069**	2.	3. RE
4. TITLE AND SUBTITLE Preferential Radon Transport Through Highly Permeable Channels in Soils		5. REPORT DATE 6. PERFORMING ORGANIZATION CODE
7. AUTHOR(S) Ronald B. Mosley		8. PERFORMING ORGANIZATION REPORT NO.
9. PERFORMING ORGANIZATION NAME AND ADDRESS See Block 12.		10. PROGRAM ELEMENT NO. 11. CONTRACT/GRANT NO. EPA P.O. 4D2920NASA
12. SPONSORING AGENCY NAME AND ADDRESS **EPA, Office of Research and Development Air Pollution Prevention and Control Division Research Triangle Park, NC 27711**		13. TYPE OF REPORT AND PERIOD COVERED Published paper; FY94-FY95 14. SPONSORING AGENCY CODE **EPA/600/13**

15. SUPPLEMENTARY NOTES APPCD project officer is Ronald B. Mosley, E305-03, 919/541-7865. For presentation at the 7th Int. Symp. on the Natural Radiation Environment (NRE-VII), Rhodes, Greece, 5/20-24/02).

16. ABSTRACT

The paper discusses preferential radon transport through highly permeable channels in soils. Indoor radon levels (that can pose a serious health risk) can be dramatically increased by air that is drawn into buildings through pipe penetrations that connect to permeable channels in soils. The channels, commonly containing gravel bedding around utility pipes, act as a collecting plenum for soil radon and can draw air from distances approaching 100 m. Equations characterizing air and radon flow in such channels are developed and compared with field data in this paper. This pollutant entry mechanism has recently attracted new attention because of its relevance to entry of volatile organic compounds from contaminated groundwater, leaking storage tanks, landfills, and other sources of soil vapor contamination. Three test channels were constructed to simulate conditions associated with utility line installations. Site sampling characterized soil radium, emanation, moisture, particle size, density, specific gravity, permeability, and diffusion coefficient properties. Experiments, in which air was extracted through the suction tube, showed that pressures and air flow rates decreased exponentially with distance along each channel, as predicted. Radon concentrations in the channels were lower than in surrounding soil because of their greater porosity and reduced radon source strengths.

17. KEY WORDS AND DOCUMENT ANALYSIS

a. DESCRIPTORS		b. IDENTIFIERS/OPEN ENDED TERMS	c. COSATI Field/Group	
Pollution	Ground Water	Stationary Sources	13B	08H
Radon	Storage Tanks	Indoor Air Quality	07B	13D,15E
Organic Compounds	Earth Fills		07C	13C
Volatility			20M	
Buildings			13M	
Soils			08G,08M	
Water				

18. DISTRIBUTION STATEMENT **Release to Public**	19. SECURITY CLASS *(This Report)* Unclassified	21. NO. OF PAGES **28**
	20. SECURITY CLASS *(This page)* Unclassified	22. PRICE

EPA Form 2220-1 (9-73)